Article:
Li, G., Zhang, K., Zhu, Z.Q. et al. (2018) Comparative studies of torque performance improvement for different doubly salient synchronous reluctance machines by current harmonic injection. IEEE Transactions on Energy Conversion. ISSN: 0885-8969

https://doi.org/10.1109/TEC.2018.2870753

Comparative Studies of Torque Performance Improvement for Different Doubly Salient Synchronous Reluctance Machines by Current Harmonic Injection

G. J. Li, *Senior Member*, *IEEE*, K. Zhang, Z. Q. Zhu, *Fellow*, *IEEE*, and G. W. Jewell

***Abstract*—Three types of doubly salient synchronous reluctance machines have been comparatively studied to improve the torque performance using current harmonic injection methods. These machines are derived from the switched reluctance machines (SRMs) with different winding configurations, such as the double/single layer mutually coupled SRMs (MCSRMs) and fully pitched SRMs (FPSRMs), by supplying them with sinewave current. Such current supply mode can lead to higher torque/power density, lower vibrations and acoustic noise compared to the conventional rectangular current supply. The proposed torque analytical model can predict the instantaneous torque of the doubly salient SRMs with sinewave current excitation and the current harmonics also can be selected in order to reduce the torque ripple and/or increase the average torque. It has been found that the 3rd current harmonic injection shows the best performance for single-layer MCSRMs and FPSRMs because it improves the average torque and reduces the torque ripple at the same time. However, it has little influence on doubly-layer MCSRMs. To improve the torque performance of such machines, other harmonic currents, e.g. 5th and 7th, need to be used. Both static and dynamic tests have been carried out to validate the predictions.**

***Index Terms*—Current harmonic injection, switched reluctance machine, synchronous reluctance machine, torque ripple reduction.**

NOMENCLATURE

SRM	Switched/synchronous reluctance machine
MC	Mutually coupled
FP	Fully pitched
SL	Single layer winding
DL	Double layer winding

I. INTRODUCTION

SWITCHED reluctance machines (SRMs) are stepper motors which only produce the reluctance torque and were first presented by Robert Davidson in 1838 [1]. With the rapid development in industry, SRMs have gained a substantial foothold in harsh environment and safety-critical applications. Without permanent magnets and windings on the rotor, it can reduce the system costs and also avoid the problems associated with permanent magnets such as the irreversible demagnetization [2]. In particular, their simple and robust structure, high manufacturability, good fault tolerance and high speed and temperature operation capabilities brought them the powerful competitiveness for automotive and aerospace applications [3]. However, the doubly salient structure leads to inherent drawbacks, such as high torque ripple, vibrations and acoustic noise, which significantly limit their market penetration into sectors that are sensitive to these issues. As a result, torque ripple and vibration mitigations for SRMs become some of the most important research topics in literature.

Recently, many researchers investigated the possibility of reducing the vibrations and acoustic noise of conventional SRMs by using sinewave current supply rather than the classic rectangular wave current supply (120 electrical degrees conduction for 3-phase SRMs). This in effect makes SRMs become the doubly salient synchronous reluctance machines, as investigated in [4-7]. It has been found that the sinewave current supply has significant benefits on the radial force excitation reduction, which is the primary source of the vibrations and acoustic noise [8]-[9]. However, the torque capability with sinewave current supply is reduced compared with the rectangular wave current supply [10]. In order to increase the average torque, the researchers in [11] [12] have proposed a new class of SRMs with fully pitched windings, namely fully pitched SRMs (FPSRMs). The torque generation of FPSRMs is entirely due to the rate of change of mutual-inductances between phases. It was verified that with sinewave current supply, FPSRMs can produce a torque twice as high as that of conventional SRMs. However, their longer end-winding compared with the short pitched winding of conventional SRMs results in higher copper loss at the same current level.

To combine the advantages of both conventional SRMs (short end-winding) and FPSRMs (high torque capability), the mutually coupled SRMs (MCSRMs) with double layer windings (DL) have been proposed in [13] [14]. It has been established that the double layer MCSRMs generate torque via variation of both the self- and mutual-inductances, and are less sensitive to the magnetic saturation. As a result, the double layer MCSRMs can operate at higher phase current and achieve higher overload capability [10] [15]. Apart from the aforementioned benefits, the double layer MCSRMs can also

The authors are with the Electrical Machines and Drives Group, The University of Sheffield, Sheffield, S1 3JD, UK, (e-mail: g.li@sheffield.ac.uk; kzhang8@sheffield.ac.uk; z.q.zhu@sheffield.ac.uk; g.jewell@sheffield.ac.uk).

achieve lower vibration and acoustic noise compared to conventional SRMs [16]. However, due to the nature of the self-and mutual-inductance variations, the torque ripple of double layer MCSRMs is also higher. In order to mitigate this issue, researchers in [10] proposed some MCSRMs with single layer windings (SL). They exhibit better performance, e.g. higher average torque and also lower torque ripple, at low current conditions compared to their double layer counterparts. However, these advantages diminish with increasing saturation level.

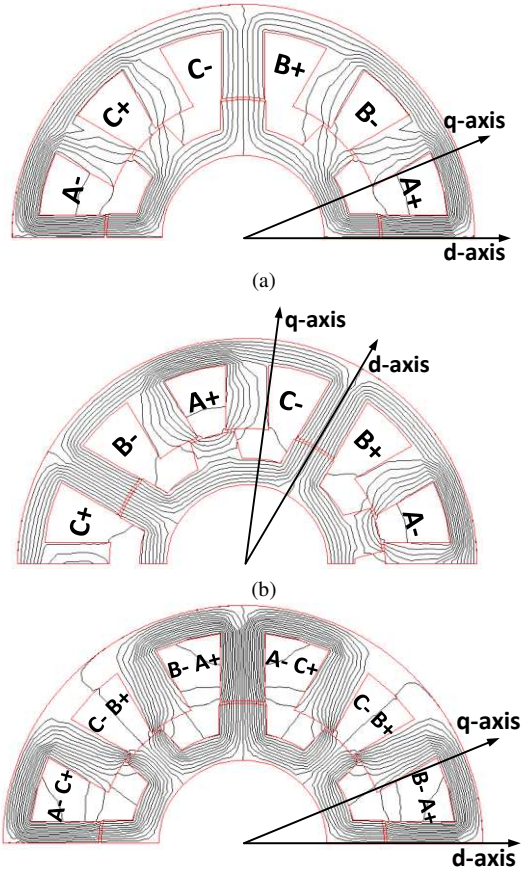

Fig. 1 Comparison of flux distribution at aligned position when the phase A is supplied by a 1A dc current. (a) Single layer MCSRMs, (b) FPSRMs, (c) double layer MCSRMs.

TABLE I. MACHINE LEADING DIMENSIONS AND DESIGN FEATURES

Stator slot number	12	Rotor inner radius (mm)	15.7
Rotor pole number	8	Rotor tooth width (mm)	8.91
Stator outer radius (mm)	45	Active length (mm)	60
Stator York height (mm)	5.1	Number of turns per phase	132
Stator tooth width (mm)	8.45	Coil packing factor	0.37
Air gap length (mm)	0.5	Rated RMS current (A)	10
Rotor outer radius (mm)	26.5	Current density (A_{rms}/mm^2)	5.68

In this paper, the comparative investigations between the doubly salient synchronous reluctance machines that evolved from the aforementioned SRMs with three different winding configurations, as shown in Fig. 1, are carried out by using the proposed current harmonic injection method. For simplicity, they will still be called single/double layer MCSRMs, and FPSRMs throughout this paper. Single/double layer conventional SRMs will not be investigated due to their poor performance when supplied with sinewave current. The idea is to generate an opposite torque ripple by the injected current harmonics to compensate that produced by the fundamental current. As a result, the torque ripple can be reduced and the average torque might be increased at the same time. Without heavy saturation, the harmonic order, the phase angles and also the magnitudes of the injected current harmonics can be predicted in order to achieve the minimum torque ripple and/or maximum average torque.

II. METHODOLOGY OF CURRENT HARMONIC INJECTION

Fig. 1 shows the flux distributions at aligned position for three designed and optimized SRMs winding configurations, of which the machine parameters are given in TABLE I. Without considering the magnetic saturation, the general torque expression of SRMs can be described by

$$T_e = \frac{1}{2}i_a^2\frac{dL_a}{d\theta} + \frac{1}{2}i_b^2\frac{dL_b}{d\theta} + \frac{1}{2}i_c^2\frac{dL_c}{d\theta} + i_a i_b\frac{dM_{ab}}{d\theta} + i_a i_c\frac{dM_{ac}}{d\theta} + i_b i_c\frac{dM_{bc}}{d\theta} \quad (1)$$

where i_{abc}, L_{abc} and M_{xy} (xy is any combination of phases a, b and c) are the three phase currents, and the self- and mutual-inductances, respectively. θ is the mechanical rotor position.

Due to different winding configurations, the self- and mutual-inductances for single/double layer MCSRMs and FPSRM are different as well, which result in different electromagnetic torque contribution, as shown in TABLE II. Since the self-inductance of single layer MCSRMs is much larger than the mutual-inductance, the torque due to the self-inductance is the most dominant component. However, the torque generation of FPSRMs is entirely due to the mutual-inductances because the variation of the self-inductances can be neglected. Moreover, double layer MCSRMs combines both the benefits of the self- and mutual-inductances.

TABLE II. ELECTROMAGNETIC TORQUE COMPONENTS FOR DIFFERENT SRMS

	Torque Components	
	Dominant	Subordinate
SLMCSRM	Self-torque	Mutual-torque
DLMCSRM	Self-/Mutual-torque	-
FPSRM	Mutual-torque	Self-torque

In order to identify the contribution of certain order current harmonic to the average torque and torque ripple. The stator current with single current harmonic injection can be described by (2), and the self- and mutual-inductances can be expressed by Fourier series analysis, as shown in (3) and (4), respectively. It is worth noting that only the current and inductances of phase a are given. Other phases have the same amplitude but with a phase shift of 120°.

$$I_a = I_1\sin(\theta_e + \beta_1) + I_v\sin(v\theta_e + \beta_v) \quad (2)$$

$$L(\theta_e) = L_0 + \sum_{n=1}^{\infty} L_n\cos(n\theta_e + \alpha_n) \quad (3)$$

$$M(\theta_e) = M_0 + \sum_{n=1}^{\infty} M_n \cos(n\theta_e + \alpha'_n) \tag{4}$$

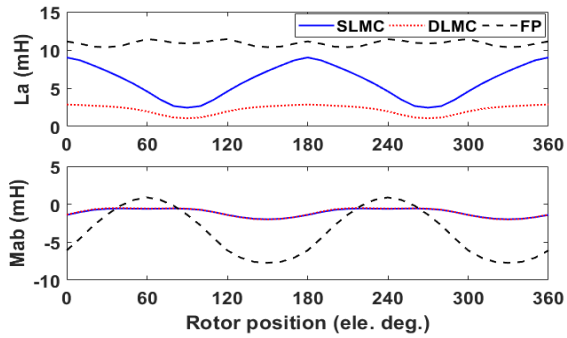

(a)

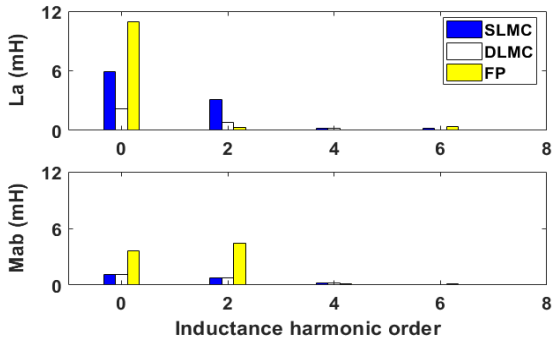

(b)

Fig. 2 Comparison of (a) inductances and (b) spectra for three winding configurations. The phase a is supplied with a 1A dc current.

The definitions of the above parameter are as follows.

1) L_0 and M_0 are the dc components of the self- and mutual-inductances; L_n and M_n represent the n^{th} order self- and mutual-inductance harmonic magnitudes; α_n and α'_n are the phase angles of the corresponding inductance harmonics. These parameters are assumed to be constant if saturation level does not change and can be calculated by using finite element analysis (FEA) and Fast Fourier Transform (FFT), as shown in Fig. 2.
2) v is the current harmonic order, such as 3rd, 5th, 7th, etc. used in this paper; I_1 and I_v express the fundamental and the v^{th} order current harmonic magnitudes; β_1 and β_v represent the phase angles of the fundamental and the injected v^{th} order harmonic currents, respectively.
3) θ_e is the rotor electrical position and n is the inductance harmonic order, such as 2nd, 4th, 6th, etc.

Substituting (2)-(4) into (1), the detailed analytical instantaneous torque model of SRMs can be obtained. More precisely, the resultant torque produced by SRMs, T_e, can be decomposed into two components: the torque produced by the fundamental current, T_f, and the one produced by the current harmonics T_h, which are given in (5).

$$T_e = T_f + T_h \tag{5}$$

with

$$T_f = T_{f0} + T_{frip} = T_{fsel} + T_{fmut} \tag{6}$$

$$T_h = T_{h0} + T_{hrip} = T_{hsel} + T_{hmut} \tag{7}$$

where '*f*' and '*h*' indicate the fundamental current and harmonic current respectively; '0' and '*rip*' represent the average component and ripple component, respectively; '*sel*' and '*mut*' represent the components due to the self- and mutual-inductances, respectively.

The detailed torque generation without current harmonic injection T_f can be simplified by (8), where k is a non-negative integer. It can be proven that the frequency of torque ripple for a 12s/8p SRM is due to the triplen harmonics. Moreover, when the number k is equal to '0', (8) could give the average torque and can be expressed as (9).

$$\begin{aligned} T_f = \frac{3p}{2}\sum_{k=0}^{\infty}\Big\{ & -\frac{3k}{2}L_{3k}I_1^2\sin(3k\theta_e + \alpha_{3k}) + \frac{3k-2}{4}I_1^2L_{3k-2}\sin(3k\theta_e + 2\beta_1 + \alpha_{3k-2}) + \frac{3k+2}{4}I_1^2L_{3k+2}\sin(3k\theta_e - 2\beta_1 + \alpha_{3k+2}) \\ & + \frac{3k}{2}I_1^2M_{3k}\sin(3k\theta_e + \alpha'_{3k}) + \frac{3k-2}{2}I_1^2M_{3k-2}\sin\left(3k\theta_e + 2\beta_1 + \alpha'_{3k-2} - \frac{2\pi}{3}\right) \\ & + \frac{3k+2}{2}I_1^2M_{3k+2}\sin\left(3k\theta_e - 2\beta_1 + \alpha'_{3k+2} + \frac{2\pi}{3}\right)\Big\} \end{aligned} \tag{8}$$

and

$$\begin{aligned} T_{f0} = & \frac{3}{4}I_1^2L_2\sin(-2\beta_1 + \alpha_2) \\ & + \frac{3}{2}I_1^2M_2\sin\left(-2\beta_1 + \alpha'_2 + \frac{2\pi}{3}\right) \end{aligned} \tag{9}$$

Furthermore, according to foregoing substitutions, the torque produced by current harmonics, T_h, can be decoupled as the sum of the self- and mutual-torques, and the details are shown in (10) and (11). Here, the torque due to the interaction between the inductance harmonics and the current harmonics (torque term $T_e(I_v{}^2)$) has been neglected due to its small magnitude.

$$\begin{aligned} T_{hsel} = \frac{3p}{2}\sum_{n=1}^{\infty}\frac{nL_n}{2}I_1I_v\{ & \sin(A\theta_e + \beta_1 + \beta_v + \alpha_n) \\ & - \sin(B\theta_e + \beta_1 + \beta_v - \alpha_n) \\ & - \sin(C\theta_e + \beta_1 - \beta_v + \alpha_n) \\ & + \sin(D\theta_e + \beta_1 - \beta_v - \alpha_n)\} \end{aligned} \tag{10}$$

and

$$T_{hmut} = \frac{3p}{2}\sum_{n=1}^{\infty}\frac{nM_n}{2}I_1I_v \left\{\sin\left(A\theta_e+\beta_1+\beta_v+\alpha'_n-\frac{2\pi}{3}v\right) -\sin\left(B\theta_e+\beta_1+\beta_v-\alpha'_n-\frac{2\pi}{3}v\right) -\sin\left(C\theta_e+\beta_1-\beta_v+\alpha'_n+\frac{2\pi}{3}v\right) +\sin\left(D\theta_e+\beta_1-\beta_v-\alpha'_n+\frac{2\pi}{3}v\right) +\sin\left(A\theta_e+\beta_1+\beta_v+\alpha'_n-\frac{2\pi}{3}\right) -\sin\left(B\theta_e+\beta_1+\beta_v-\alpha'_n-\frac{2\pi}{3}\right) -\sin\left(C\theta_e+\beta_1-\beta_v+\alpha'_n-\frac{2\pi}{3}\right) +\sin\left(D\theta_e+\beta_1-\beta_v-\alpha'_n-\frac{2\pi}{3}\right)\right\} \quad (11)$$

and

$$\begin{cases} A = 1+v+n \\ B = 1+v-n \\ C = 1-v+n \\ D = 1-v-n \end{cases} \text{ with } A,B,C,D = 0,\pm3,\pm6,\pm9\ldots \quad (12)$$

It can be proven that the frequency of T_h correlates with the current and inductance harmonic orders as shown in (12). Generally, T_h will only contain the triplen harmonics, so do T_f. This means that the combination of v and n needs to generate multiples of three for A to D. By way of example, when v is equal to 3, the term A can contribute to torque only if n is equal to 2, 5, 8, etc. If this condition satisfies, the average torque T_{h0} can then be obtained, as described by (13), where the rotor position θ_e is equal to '0'.

$$T_{h0} = -\frac{3pn}{4}I_1I_v\left[L_{v\mp1}\sin(\beta_1\mp\beta_v\pm\alpha_n) + M_{v\mp1}\sin\left(\beta_1\mp\beta_v\pm\alpha'_n\pm\frac{2\pi}{3}v\right) + M_{v\mp1}\sin\left(\beta_1\mp\beta_v\pm\alpha'_n-\frac{2\pi}{3}\right)\right] \quad (13)$$

Due to the nature of the inductances, the odd order inductance harmonics can be neglected. (8) and (9) also show that the dc inductance component has no contribution to the torque, and hence can be neglected as well. The average torque produced by the fundamental current only depends on the 2nd order inductance harmonic. However, other even order inductance harmonics contribute to the torque ripples, in which the dominant one, i.e. the 6th order torque harmonic, is produced by the 4th, 6th and 8th order inductance harmonics. As a result, in order to reduce the torque ripple, this paper is focused to reduce the 6th order torque harmonic. According to (10)-(12), the active inductance harmonics considered in this paper that contribute to the average torque and/or the torque ripple, are listed in TABLE III. It is worth noting that the 2nd order inductance harmonic plays a more significant role in the 6th order torque ripple than other inductance harmonics, due to its higher magnitude (See Fig. 2). Moreover, in order to increase the accuracy of predicting the torque ripple due to the fundamental current, the 12th order torque harmonic is also considered in this paper.

TABLE III. ACTIVE INDUCTANCE ORDER SELECTION FOR TORQUE PRODUCTION

Current Components	Average torque	6th torque ripple	12th torque ripple
Fundamental	2nd	4th, 6th, 8th	12th
3rd harmonic	2nd and 4th	2nd, 4th, 8th, 10th	-
5th harmonic	4th and 6th	2nd, 10th, 12th	-
7th harmonic	6th and 8th	2nd, 12th, 14th	-

Fig. 3 shows the prediction of on-load torque with and without the 3rd order current harmonic injection for the three aforementioned SRMs. It shows a generally good agreement between the FEA and analytically predicted results for a phase root-mean-square (RMS) current of 1A. Moreover, it can be proven that the proposed injection method can reduce the torque ripples while increasing the average torque for both single layer MCSRMs and FPSRMs, but has little effect on double layer MCSRMs. This will be investigated further in Section III. It is worth noting that with high phase current supplied, there will be a marginal discrepancy between the FE results and the analytical predictions due to magnetic saturation. However, the torque ripple can still be reduced by the proposed harmonic current injection method.

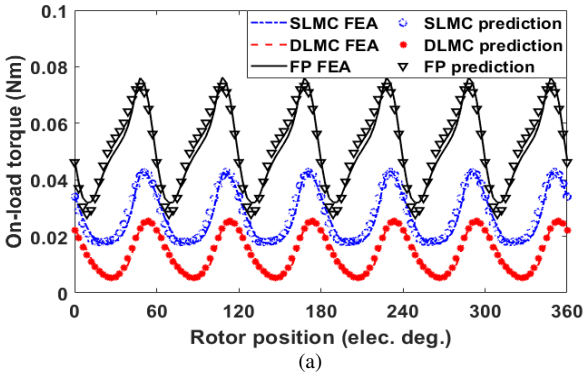

(a)

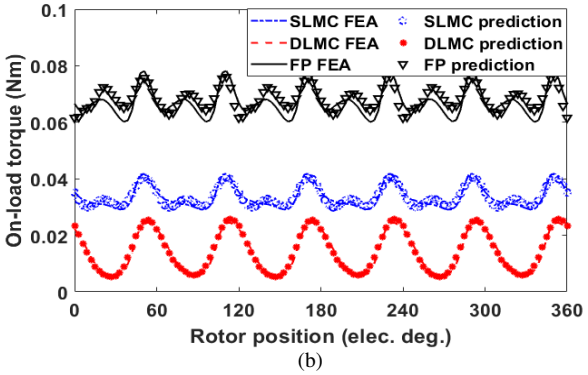

(b)

Fig. 3 Comparison of FEA and analytically predicted torque waveforms for the three SRMs when 1A RMS current is supplied. (a) Without 3rd current harmonic injection, (b) With 30% 3rd current harmonic injection.

III. Comparison of Torque Contribution with Third Current Harmonic Injection

A. Torque contribution for single/double layer MCSRMs

Using the analytical torque models derived in previous sections, the torque produced by both the fundamental and harmonic currents can be reliably predicted without considering heavy magnetic saturation. According to T_{h0} in (13), the average torque, due to current harmonics, is a function of current harmonic phase angle β_v and can be simplified by (14) based on the trigonometric function transformation.

$$T_{h0}(\beta_v) = T_{res}\sin(\beta_v + \varphi_{res}) \tag{14}$$

where T_{res} and φ_{res} are the resultant torque magnitude and phase angle, respectively. φ_{res} is a constant and can be calculated using the inductance magnitude and also phase angle. It is 1.3° and 6.1° for the single/double layer MCSRMs, respectively. It is obvious that the maximum average torque occurs when $\sin(\beta_v + \varphi_{res}) = 1$. Hence, the predicted β_v where the maximum torques can be achieved for the single/double layer MCSRM can be easily calculated as 88.7° and 83.9°, respectively, as shown in Fig. 4(a).

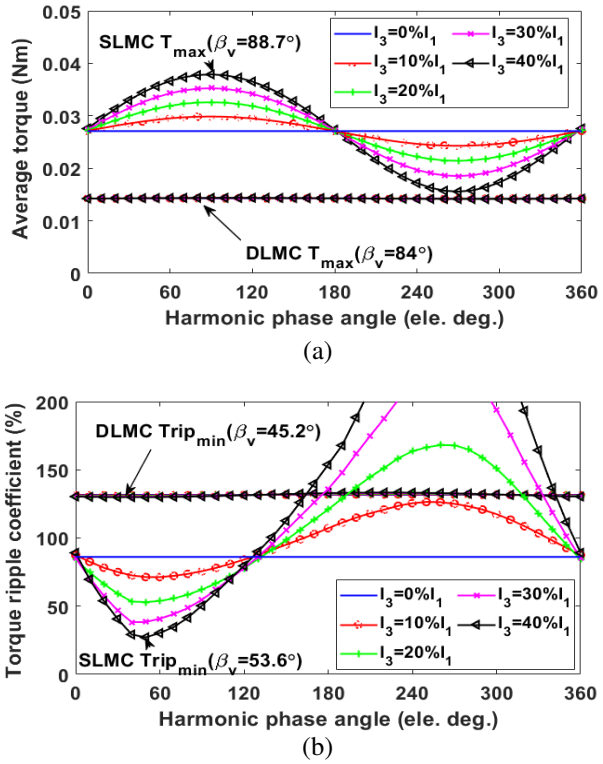

(a)

(b)

Fig. 4 FEA results of torque production for single/double layer MCSRM with the 3rd order current harmonic injection. The machines are supplied with 1A RMS current. (a) Average torque, (b) Torque ripple coefficient.

As aforementioned in Section 0, the 6th order torque ripple is the most dominant one, which is due to the fundamental and harmonic currents and can be simplified by (15) and (16) according to (8)-(12).

$$T_{frip} = T_{Frip}\,sin(6\theta_e + \varphi_{Frip}) \tag{15}$$

$$T_{hrip}(\beta_v, I_v) = T_{Hrip}(I_v)\sin(6\theta_e + \varphi_{Hrip} + \beta_v) \tag{16}$$

Therefore, the minimum torque ripple occurs when (15) and (16) have the same magnitude but π phase difference between them. This leads to (17)-(18).

$$T_{Frip} = T_{Hrip}(I_v) \tag{17}$$

$$\varphi_{Hrip} + \beta_v - \varphi_{Frip} = (2d+1)\pi \tag{18}$$

where d is an integer. Based on (8), (10) and (11), φ_{Frip} and φ_{Hrip} can be calculated as $143.5°$ and $-90.1°$, respectively, for the single layer MCSRM. Therefore, the phase angle to achieve the minimum torque ripple can be obtained as $\beta_v = 53.6°$. It is the same for the double layer MCSRM, β_v of which is 45.2°. Fig. 4(b) shows how the 3rd order current harmonic affects the torque ripple coefficients for both the single/double layer MCSRM. The torque ripple coefficient is calculated by $((T_{max} - T_{min})/T_{av})$, where T_{max}, T_{min} and T_{av} are the maximum, the minimum and the average torques for one electrical period, respectively. It can be seen that for the single layer MCSRM, the 3rd order current harmonic can reduce the torque ripple coefficient by 56% while increasing the average torque by 10%. However, whatever the 3rd order current harmonic is injected, it has little effect on both the average torque and the torque ripple coefficient of the double layer MCSRM.

In order to study the reason why this is happening, the harmonic torques due to the self- and mutual-inductances are investigated separately by using (10)-(13). The active inductance harmonics (e.g. 2nd and 4th) for the 3rd order current harmonic injection listed in TABLE III are taken into account. By way of example, T_{hrip_2nd} produced by the 2nd order inductance harmonic with the 3rd order current harmonic injected [n=2, v=3 in (13)] can be simplified as (19).

$$\begin{aligned} T_{hrip\_2nd} = \frac{3p}{2} I_1 I_3 \Big[& L_2 \sin(6\theta_e + \beta_1 + \beta_3 + \alpha_2) + \\ & M_2 \sin\left(6\theta_e + \beta_1 + \beta_3 + \alpha'_2 - \frac{\pi}{3}\right)\Big] \end{aligned} \tag{19}$$

From the observation of the inductances, it is found that α_2 leads α'_2 by around $2\pi/3$ for both the single/double layer MCSRM, which means $\alpha_2 - \alpha'_2 \approx 2\pi/3$ is always valid. As a result, the harmonic torque components in T_{hrip_2nd} due to the self- and mutual-inductances will produce a π phase difference for any 3rd order current harmonic injections as shown in (20).

$$\begin{aligned} T_{hrip\_2nd} &\approx \frac{3p}{2} I_1 I_3 [L_2 \sin(6\theta_e + \beta_1 + \beta_3 + \alpha_2) \\ &\quad + M_2 \sin(6\theta_e + \beta_1 + \beta_3 + \alpha_2 - \pi)] \\ &\approx \frac{3p}{2} I_1 I_3 (L_2 - M_2)\sin(6\theta_e + \beta_1 + \beta_3 + \alpha_2) \end{aligned} \tag{20}$$

Together with the similar magnitudes of L_2 and M_2 for the double layer MCSRM, T_{h0_2nd} will be cancelled to a negligible level. The elimination happens on both average torque and torque ripple, which can be clearly shown in Fig. 5(b). For comparison, Fig. 5(a) shows the harmonic torque composition for the single layer MCSRM. Even though its self- and mutual-torques still have opposite signs, the larger difference between L_n and M_n leads to the considerable contribution in both the average torque and the torque ripple. This explains why the 3rd order current harmonic injection has little effect on

the double layer MCSRM but can improve the torque performance for the single layer MCSRM.

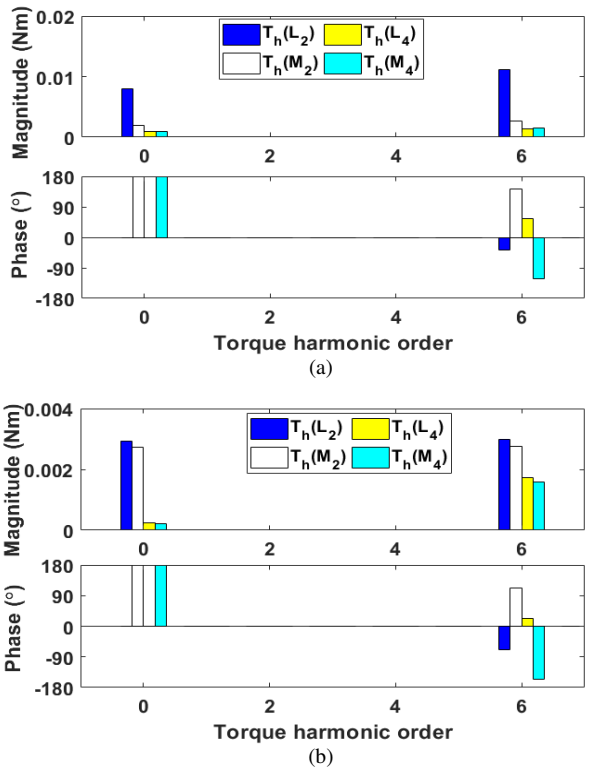

Fig. 5 Spectra of the harmonic torque produced by the active inductances with 30% 3rd current harmonic injection. The machines are supplied with 1A RMS current. (a) Single layer MCSRM (b) Double layer MCSRM.

B. Torque contribution for FPSRM

As well-established in [11] [13] and [17], the torque generation of the FPSRM depends entirely on the mutual inductance variation. This is the same case for the harmonic torque generation. The 2nd order self-inductance harmonic of the FPSRM is too small to produce any meaningful average torque, which can be predicted by (10)-(13), also shown in Fig. 6. However, due to a significant 2nd order mutual-inductance harmonic, there is a good potential for the FPSRM to improve its torque performance (increased average torque and reduced torque ripple) by injecting the 3rd order current harmonic.

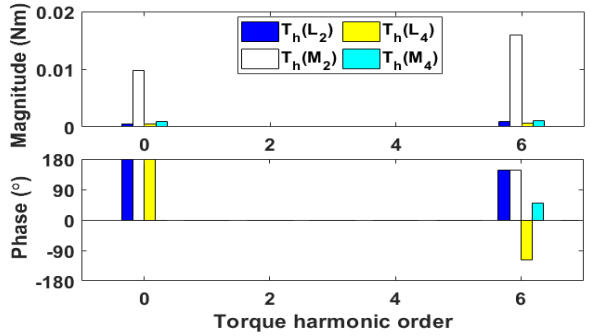

Fig. 6 Spectra of the harmonic torque produced by the active inductance harmonics with 30% 3rd order current harmonic injection for the FPSRM. The machines are supplied with 1A RMS current.

By using the same analytical torque model, the average torque and torque ripple coefficient against current harmonic phase angle for the FPSRM can be obtained, as shown in Fig. 7. The optimization of average torque and torque ripple can be carried out by applying the same equations (14)-(18) and the optimal 3rd order current harmonic phase angles are selected as 268.7° and 270.6°, respectively.

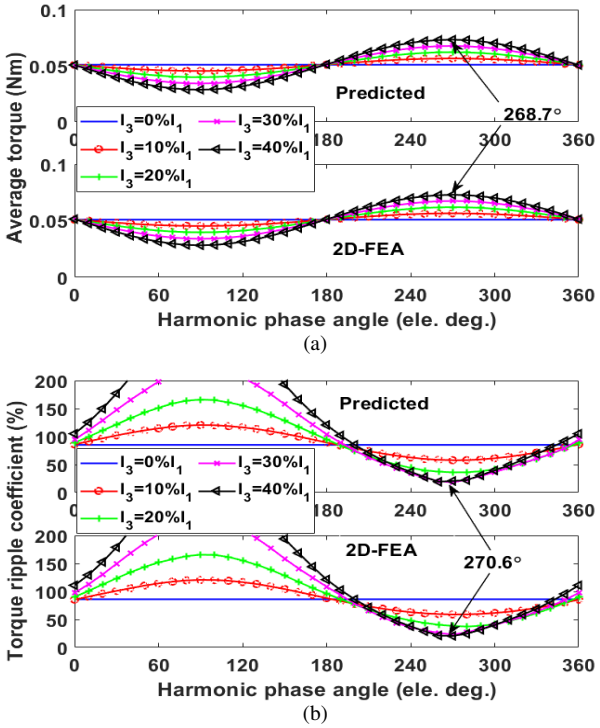

Fig. 7 Comparison between the 2D-FEA results and the analytical predictions for the FPSRM with the 3rd order current harmonic injection when three phases are supplied with 1A RMS currents. (a) Average torque, (b) Torque ripple coefficient.

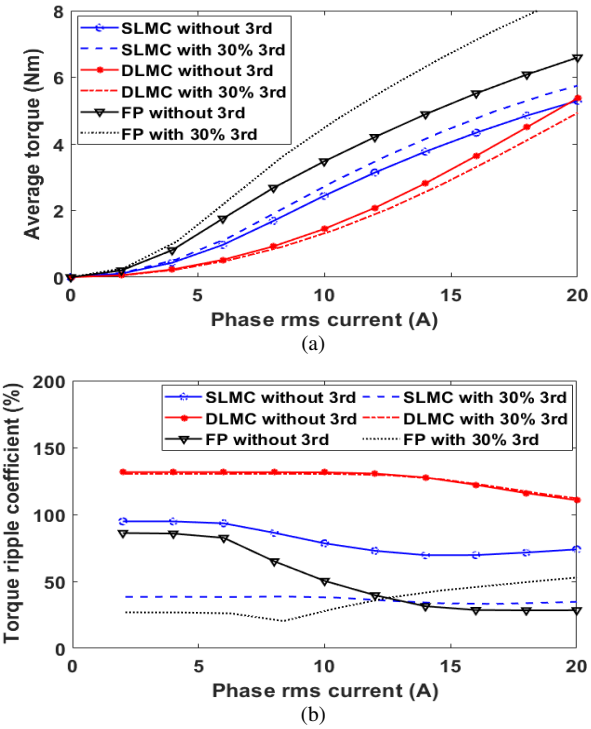

Fig. 8 Comparison of (a) average torque and (b) torque ripple coefficient versus phase RMS current with/without the 3rd order current harmonic injection. The phase angle is selected at which the minimum torque ripple occurs (53.6° for the single layer MCSRM, 45.2° for the double layer MCSRM and 270.6° for the FPSRM).

C. Torque performance with saturation consideration

The machine inductances can vary nonlinearly with respect to phase RMS currents due to magnetic saturation. Therefore, this section investigates the influence of magnetic saturation on the effectiveness of the 3rd order current harmonic injection for different electric loadings. The comparison in terms of average torque and torque ripple coefficient against phase RMS current have been calculated by FEA, as shown in Fig. 8.

As can be found, for both the single layer MCSRM (dominant self-torque) and the FPSRM (pure mutual-torque), the 3rd order current harmonic could minimize the torque ripple and increase the average torque at lower current level. With increasing current density, the 3rd order current harmonic can still increase the average torque for the FPSRM by about 25% but it loses the benefit in torque ripple reduction. One of the important reasons is that the machine inductances cannot be calculated accurately under magnetic saturation condition without using frozen permeability [14] [18]. This means that the current harmonics can no longer be properly selected by the proposed analytical torque model. Moreover, the 3rd order current harmonic injection has little effect on the double layer MCSRM (self- and mutual torques) as investigated previously. The slight reduction in the average torque is due to the fact that for the same RMS current, the additional injected 3rd order harmonic current leads to a reduced fundamental current.

IV. Fifth and Seventh Order Harmonic Current Injections

The proposed analytical torque model could also be implemented to other orders of current harmonic injections, such as the 5th and 7th order current harmonics. It is worth mentioning that the even order current harmonics always present undesirable torque performance (reduced average torque and increased torque ripple), hence will not be detailed in this paper.

In order to investigate the torque contribution for the 5th and 7th order current harmonics, the analytical method for the 3rd order current harmonic has been implemented for the three investigated machines as well. By way of example, for the double layer MCSRM, when the 5th order current harmonic (v=5) is injected, according to (10)-(12) and TABLE III, the dominant 6th order torque ripple ($|D|$=1-v-n=6), produced by the 2nd order inductance harmonic (n=2), can be expressed as (21).

$$T_{hrip\_2nd} = -\frac{3p}{2} I_1 I_5 \left[L_2 \sin(-6\theta_e + \beta_1 - \beta_5 - \alpha_2) + 2M_2 \sin\left(-6\theta_e + \beta_1 - \beta_5 - \alpha'_2 - \frac{2\pi}{3}\right)\right] \quad (21)$$

As aforementioned, $\alpha_2 - \alpha'_2 \approx 2\pi/3$ for the double layer MCSRM is again valid. Substituting it into (21) leads to

$$\begin{aligned} T_{hrip\_2nd} &\approx -\frac{3p}{2} I_1 I_5 [L_2 \sin(-6\theta_e + \beta_1 - \beta_5 - \alpha_2) \\ &\quad + 2M_2 \sin(-6\theta_e + \beta_1 - \beta_5 - \alpha_2)] \\ &\approx -\frac{3p}{2} I_1 I_5 (L_2 + 2M_2) \sin(-6\theta_e + \beta_1 - \beta_5 - \alpha_2) \end{aligned} \quad (22)$$

It is obvious that the self- and mutual-torque ripples due to the 5th order current harmonic will always have the same phase angle. This is different from that of the 3rd order current injection, and they will add together to compensate the torque ripple produced by the fundamental current, leading to an overall reduced torque ripple. As shown in Fig. 9, it will happen for the 7th order current harmonic injection as well. As a result, the 5th and 7th order current harmonics can achieve much more significant torque ripple reduction than that of the 3rd order current harmonic for the double layer MCSRM.

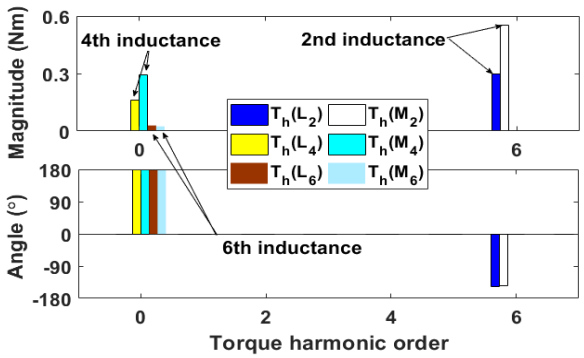

Fig. 9 Spectra of the harmonic torques produced by active inductance harmonics with 30% 5th order current harmonic injection. The double layer MCSRM are supplied with 1A RMS current.

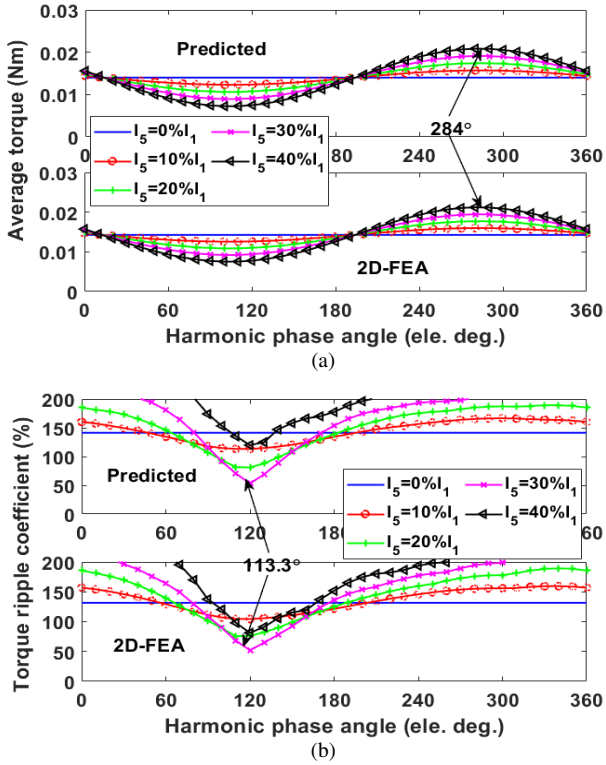

Fig. 10 Comparison between the FEA results and the analytical prediction for the double layer MCSRM with the 5th order current harmonic injection when three phases are supplied with 1A RMS current. (a) Average torque, (b) Torque ripple coefficient.

Moreover, the torque production improvement with respect to the 5th order current harmonic phase angle for the double layer MCSRM is shown in Fig. 10. It is apparent that the torque behavior with the 5th order current harmonic injection can also be reliably predicted. The phase angles for achieving the maximum average torque and minimum torque ripple have been calculated, being 284° and 113.3° , respectively. However, different from the 3rd order current harmonica

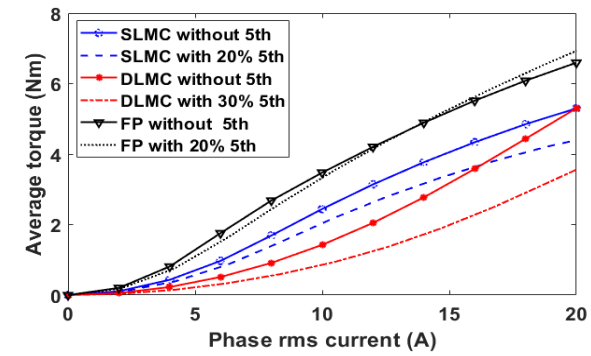

(a)

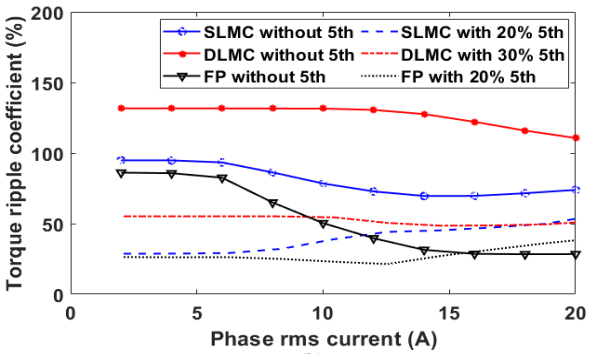

(b)

Fig. 11 Comparison of (a) average torque and (b) torque ripple coefficent with/without the 5th order current harmonic injection.

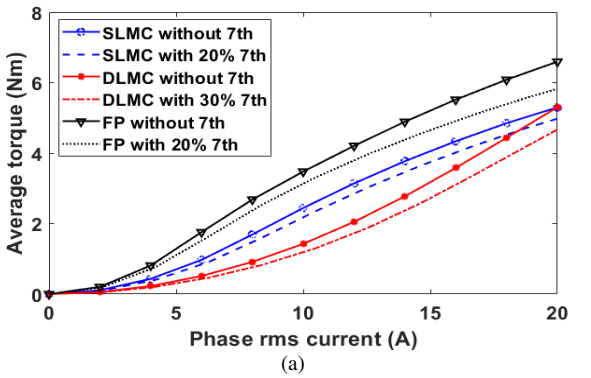

(a)

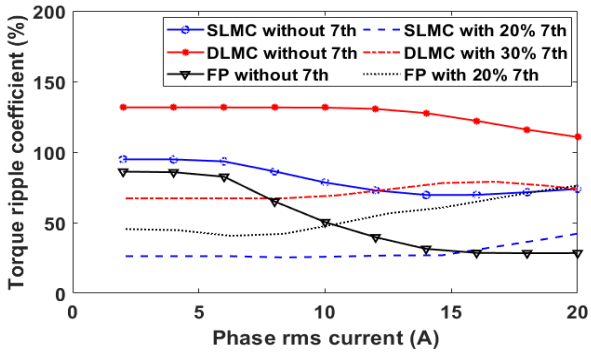

(b)

Fig. 12 Comparison of (a) average torque and (b) torque ripple coefficent with/without the 7th order current harmonic injection.

injection used for the single layer MCSRM and the FPSRM, the torque ripple and the average torque cannot be improved at the same time.

Similar investigations have been carried out for the 7th order current harmonic injection. In order to achieve the minimum torque ripple, the magnitudes and phase angles of different current harmonics are predicted and compared, as shown in TABLE IV.

TABLE IV. CHARACTERISTICS OF CURRENT HARMONIC FOR ACHIEVING MINIMUM TORQUE RIPPLE

	3rd harmonic		5th harmonic		7th harmonic	
	Mag.	Phase	Mag.	Phase	Mag.	Phase
SL-MCSRM	30%	53.6°	20%	143.6°	20%	233.4°
DL-MCSRM	30%	45.2°	30%	113.3°	30%	205.7°
FPSRM	30%	270.6°	20%	180.5°	20%	270.5°

According to the predictions in TABLE IV, the FEA results with the desired magnitude and also phase angle for achieving minimized torque ripple by the 5th order current harmonic injection are shown in Fig.11. As can be seen, the FPSRM shows the best performance with the 5th order current harmonic injection, which reduces the torque ripple by around 69% without heavy magnetic saturation. Its average torque is only marginally influenced. There are also 70% and 58% reductions in the torque ripples for the single/double layer MCSRM, respectively. However, the average torques for these two MCSRMs are also reduced by about 15% and 35%, respectively.

Similarly, the results for the 7th order current harmonic injections are shown in Fig. 12. It shows that there is around 10% reduction in average torque for all three types of machines. However, the torque ripple coefficient of the single layer MCSRM has been significantly reduced by around 72%, and the reduction is not really compromised with the increasing phase current. For the double layer MCSRM, the torque ripple coefficient can also be reduced by around 50%. Moreover, although there are 50% reduction in torque ripple coefficient for the FPSRM at low current, the benefits are compromised with increasing phase current due to magnetic saturation. The reason lies in the inaccurate calculation of machine inductances at high phase current.

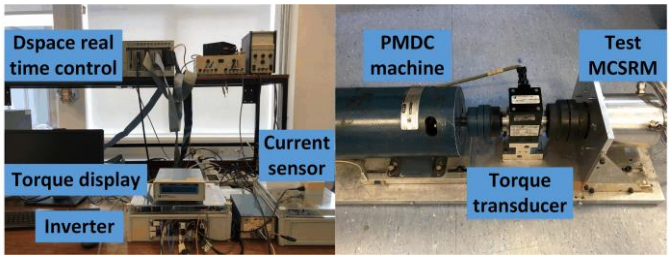

Fig. 13 Test rig for harmonic injection.

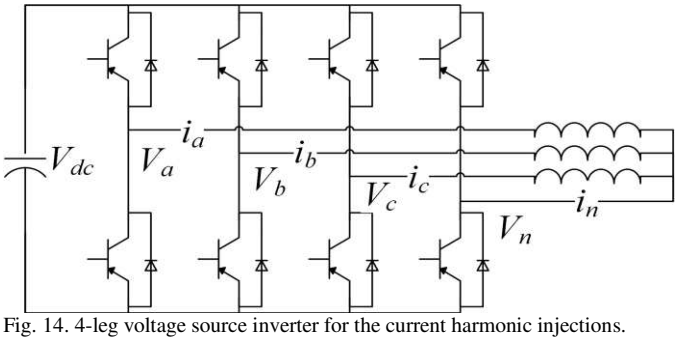

Fig. 14. 4-leg voltage source inverter for the current harmonic injections.

V. Experimental Validation

The proposed method for torque ripple reduction is validated on a prototype double layer MCSRM, which is proposed and built in [10]. The test rig is given in Fig. 13, which consists of a permanent magnet generator (load machine), a torque transducer and the test MCSRM. In the following sections, the implementation process of the current harmonic injection is first presented. Then the static and dynamic tests are carried out to evaluate the proposed approach.

A. Current harmonic implementation

Based on the Park transformation, the current harmonic injection in *dq0*-axis is investigated, as shown in Fig. 15. The *dq0*-axis reference currents are obtained from the torque controller and *dq0*-axis harmonic components are predicted by the proposed approach.

The detailed injection method is provided in TABLE V. By way of example, if one wants to inject the triplen current harmonics in the abc-reference frame, e.g. 3rd, then i_{dh} and i_{qh} need to be 0 and only i_{0h} will be injected. The parameters for i_{0h}, e.g. $v = 3$ $(k = 1)$, i_{3rd} and α_{3rd}, can be calculated in advance.

TABLE V. Implementation Of Current Harmonic Injections In DQ-axis Frame

i_{dq0h} / i_{abch}	i_{dh}		i_{qh}		i_{0h}	
	Mag.	Phase	Mag.	Phase	Mag.	Phase
$3k$	0	-	0	-	i_{3k}	α_{3k}
$3k-1$	i_{3k}	α_{3k}	i_{3k}	$\alpha_{3k}+\pi$	0	-
$3k+1$	i_{3k}	α_{3k}	i_{3k}	α_{3k}	0	-

Note: k = 1, 2, 3… abc frame harmonic orders are $3k$, $3k-1$ or $3k+1$, while in *dq0*-axis frame, they are either 0 or $3k$.

It is worth noting that the 3rd order current harmonic cannot be injected directly by the conventional 3-leg inverter, due to the fact that the zero-sequence current is not null. As a result, a 4-leg inverter, as shown in Fig. 14, has been adopted in order to inject such harmonic current. In addition, the 3-dimension space vector pulse width modulation (3D-SVPWM) is utilized to achieve zero-sequence current control [19] [20].

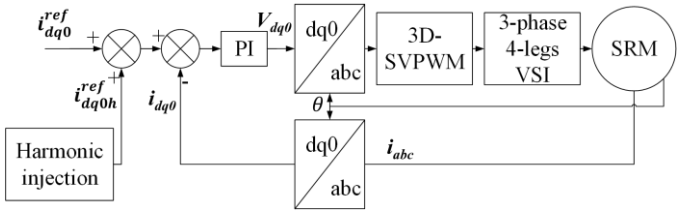

Fig. 15. Schematic control block diagram for implementing the current harmonic injection by using the 4-leg voltage source inverter.

B. Static test

The measurement of static torque of the MCSRM is implemented by using the forgoing 4-leg inverter. The rotor of the test machine is locked physically. By changing the locked rotor position and supplying three phase DC currents (amplitudes of DC currents are chosen according to 3-phase sinewave currents at different rotor positions) into the machine, the sinewave current supply can be simulated. The three phase currents can be regulated by PI controllers. In order to avoid overheating, the phase RMS current is kept at 4A during the static test. Fig. 16 shows a good agreement between the predicted and measured instantaneous torque when various current harmonics are injected.

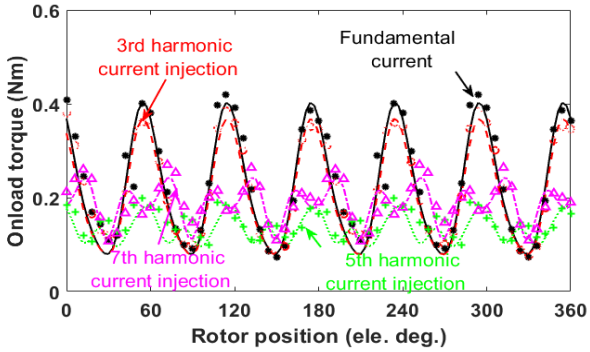

Fig. 16. Static torque versus rotor position. The MCSRM is supplied with a RMS current of 4A. (Line: prediction, marks: measurement).

C. Dynamic test

In dynamic test, the performance of current injection method at steady state is validated. The machine is operating under current control and maximum torque per ampere control ($i_d = i_q$) [10]. The phase RMS current is kept at 5A and the harmonic orders listed in TABLE IV have been adopted. Fig. 17 shows the current and torque waveforms at the steady state after the 3rd, 5th and 7th order current harmonics individually injected into the test machine, respectively. It is obvious that for the MCSRM, the 3rd order current harmonic has little effect on the torque production, as predicted. The slight reduction in *dq*-current and average torque, after the 3rd order current injection, is mainly due to the fact that the phase RMS current is kept constant. It also proves that the 5th and 7th order current harmonics can effectively reduce the speed and torque ripple.

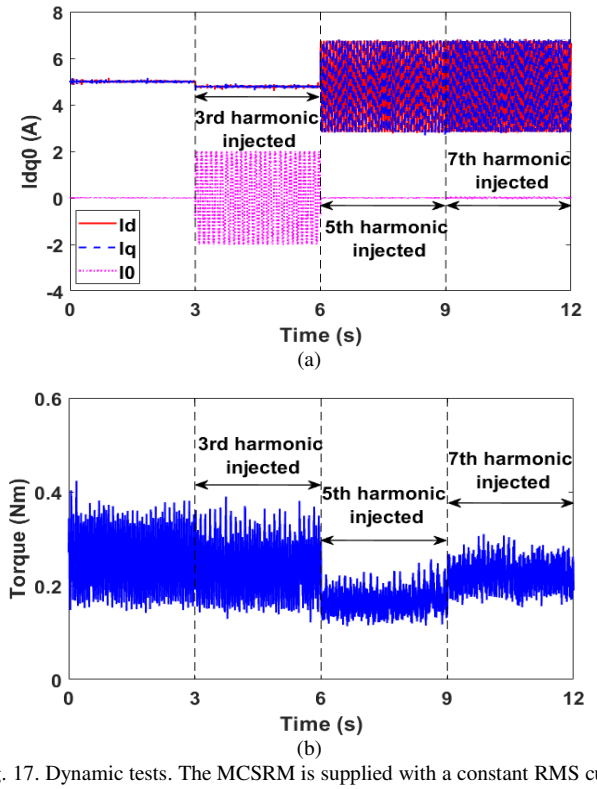

Fig. 17. Dynamic tests. The MCSRM is supplied with a constant RMS current of 5A. (a) *dq0*-axis current and (b) torque waveforms.

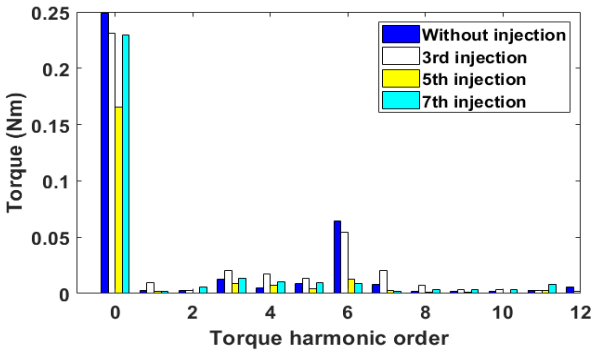

Fig. 18. Spectra of torque before and after current harmonic injection for the MCSRM.

The torque spectra are also plotted, as shown in Fig. 18. The results show that the 5th and 7th current harmonic injections can reduce 66% and 70% of the 6th order torque harmonics, respectively. The 3rd current harmonic has negligible effect on the 6th order torque harmonic. It is worth noting that the low frequency harmonics in on-load torque are mainly due to the unavoidable mechanical imbalance in test rig and also the inherent torque ripple of the load generator.

VI. Conclusion

This paper comparatively studied the torque performance improvement for three types of doubly salient synchronous reluctance machines with different windings by current harmonic injections. The proposed methods could clearly quantify the torque contribution for each inductance harmonic. Based on the analytical model, the torque behaviors after injecting current harmonics can be predicted and verified by FEA and experiments.

It has been found that the 3rd order current harmonic injection for the single layer MCSRM and the FPSRM exhibits the best performance, which can increase the average torque by 10% and 22%, respectively, while reducing the torque ripple coefficient by more than 55%. However, it has little effect on the double layer MCSRM. This is mainly because the harmonic torques due to the self- and mutual-inductances have been cancelled, leading to a negligible resultant harmonic torque.

The 5th and 7th order current harmonic injections are also implemented. The results showed that they can reduce the torque ripple coefficient of the double layer MCSRM by 56% and 50%, respectively. For the single layer MCSRM, the 7th order current harmonic injection presents better performance, which reduces the average torque by 10% but achieves 72% reduction in torque ripple coefficient. It is worth noting that all the current harmonic injection methods proposed in this paper can reduce the torque ripple for the FPSRM under light load conditions. However, due to magnetic saturation, the effect in torque ripple coefficient reduction might be compromised but average torque could still be increased. The effectiveness of the proposed current harmonic injection method has been validated by both the static and dynamic tests.

References

[1] T. Miller, "Switched reluctance motors and their control," *New York: Oxford University Press,* Jul. 1993.

[2] T. J. E. Miller, "Optimal design of switched reluctance motors," *IEEE Trans. Ind. Electron.,* vol. 49, no. 1, pp. 15-27, Feb. 2002.

[3] C. Sahin, A. E. Amac, M. Karacor, and A. Emadi, "Reducing torque ripple of switched reluctance machines by relocation of rotor moulding clinches," *IET Elec. Power Appl.,* vol. 6, no. 9, pp. 753-760, Nov. 2012.

[4] C. M. Spargo, B. C. Mecrow, J. D. Widmer, C. Morton, and N. J. Baker, "Design and validation of a synchronous reluctance motor with single tooth windings," *IEEE Trans. Energy Convers.,* vol. 30, no. 2, pp. 795-805, Jun. 2015.

[5] C. M. Spargo, B. C. Mecrow, J. D. Widmer, and C. Morton, "Application of fractional-slot concentrated windings to synchronous reluctance motors," *IEEE Trans. Ind. Appl.,* vol. 51, no. 2, pp. 1446-1455, Mar.-Apr. 2015.

[6] C. M. Donaghy-Spargo, B. C. Mecrow, and J. D. Widmer, "On the influence of increased stator leakage inductance in single-tooth wound synchronous reluctance motors," *IEEE Trans. Ind. Electron.,* vol. 65, no. 6, pp. 4475-4482, Jun. 2018.

[7] C. M. Donaghy-Spargo, "Electromagnetic–mechanical design of synchronous reluctance rotors with fine features," *IEEE Trans. Mag.,* vol. 53, no. 11, pp. 1-8, Nov. 2017.

[8] F. C. Lin and S. M. Yang, "Instantaneous shaft radial force control with sinusoidal excitations for switched reluctance motors," *IEEE Trans. Energy Convers.,* vol. 22, no. 3, pp. 629-636, Sep. 2007.

[9] X. Liu, Z. Q. Zhu, M. Hasegawa, A. Pride, and R. Deodhar, "Investigation of PWMs on vibration and noise in SRM with sinusoidal bipolar excitation," *Proc. 21th IEEE International Symposium on Ind. Electron., Hangzhou, China,* pp. 674-679, May 28-31 2012.

[10] X. Y. Ma, G. J. Li, G. W. Jewell, Z. Q. Zhu, and H. L. Zhan, "Performance comparison of doubly salient reluctance machine topologies supplied by sinewave currents," *IEEE Trans. Ind. Electron.,* vol. 63, no. 7, pp. 4086 - 4096, Jul. 2016.

[11] B. C. Mecrow, "Fully pitched-winding switched-reluctance and stepping-motor arrangements," *IET Elect. Power Appl.,* vol. 140, no. 1, pp. 61-70, Jan. 1993.

[12] B. C. Mecrow, "New winding configurations for doubly salient reluctance machines," *IEEE Trans. Ind. Appl.,* vol. 32, no. 6, pp. 1348-1356, Nov. 1996.

[13] G. J. Li, X. Ojeda, S. Hlioui1, E. Hoang, M. Gabsi, and C. Balpe, "Comparative study of switched reluctance motors performances for two current distributions and excitation modes," *In Proc. IEEE Ind. Electron. Conf. (IECON'09), Porto, Portugal,* Nov. 2009.

[14] G. J. Li, Z. Q. Zhu, X. Y. Ma, and G. W. Jewell, "Comparative study of torque production in conventional and mutually coupled SRMs using frozen permeability," *IEEE Trans. Magn.,* vol. 52, no. 6, Jun. 2016.

[15] X. Ma, G. J. Li, Z. Q. Zhu, G. W. Jewell, and J. Green, "Investigation on synchronous reluctance machines with different rotor topologies and winding configurations," *IET Elect. Power Appl.,* vol. 12, no. 1, pp. 45-53, Jan. 2018.

[16] X. B. Liang, G. J. Li, J. Ojeda, M. Gabsi, and Z. X. Ren, "Comparative study of classical and mutually coupled switched reluctance motors using multiphysics finite-element modeling," *IEEE Trans. Ind. Electron.,* vol. 61, no. 9, pp. 5066-5074, Sep. 2014.

[17] X. Y. Ma, G. J. Li, G. Jewell, and Z. Q. Zhu, "Comparative study of short-pitched and fully-pitched SRMs supplied by sine wave currents," *in Proc. Int. Conf. Ind. Technol. (ICIT'15), Seville, Spain,,* pp. 664-670, Mar. 2015.

[18] W. Q. Chu and Z. Q. Zhu, "Average torque separation in permanent magnet synchronous machines using frozen permeability," *IEEE Trans. Magn.,* vol. 49, no. 3, pp. 1202-1210, Mar. 2013.

[19] R. Zhang, V. H. Prasad, D. Boroyevich, and F. C. Lee, "Three-dimensional space vector modulation for four-leg voltage-source converters," *IEEE Trans. Power Electron.,* vol. 17, no. 3, pp. 314-326, May 2002.

[20] A. Kouzou, M. O. Mahmoudi, and M. S. Boucherit, "A new 3D-SVPWM algorithm for four-leg inverters," *Proc. IEEE Int. Ele. Mach. & Dri. Conf. (IEMDC),* pp. 1674-1681, 3-6 May 2009.